

# **Simulation of Plasma Spectra and Images of Foil Targets Using the Prism SPECT3D Radiation-Transport Post-Processor**

Binghai Ling

Advisor: Reuben Epstein

**Laboratory for Laser Energetics**  
University of Rochester

Summer High School Research Program  
2000

## **Abstract**

Modeling spectra for certain experiments is helpful in determining what occurs inside an Inertial Confinement Fusion (ICF) experiment. At the high temperatures of ICF, many of an element's outer shell electrons are lost, and absorption spectra of the L-shell and K-shell series appear. Using modeling by the PRISM Spect3D<sup>1</sup> Radiation-Transport Post-Processor on DRACO<sup>2</sup> hydrodynamic simulations, spectra and the images irradiated targets can be modeled. The images of the target will show the relative optical depth of the whole material, and the spectra can show the temperature range of a doped region.

## **Introduction**

Atomic spectroscopy of ICF is used to determine the conditions inside the target. Such information can tell physicists what needs to be done to improve the conditions of stability, confinement time, and temperature. Spect3D, a radiation-transport post-processor, uses multi-dimensional hydrodynamic output to simulate the absorption and emission of the plasma and models images and spectra of the experiment. Earlier, without Spect3D, only one-dimensional hydro output could be analyzed at LLE to produce simulated spectra.

From Spect3D output, the backlit images of the simulation show the relative optical depth of the material. From the amount of flux coming through the material and the dimensions of the target plasma, the opacity and the emissivity of the target can be

determined through calculations. In the course of this project, images were used to compare the completeness of different atomic models to a tabulated atomic model.

Space-integrated, time-resolved spectra can show the temperature range and the areal density<sup>3</sup> of the materials used. Streak-camera absorption spectra are obtained from experiments done by the OMEGA laser,<sup>4</sup> while space-integrated, time-resolved spectra are obtained from Spect3D. From the observed spectra, the temperature range of the target at a specific point in time can be determined from a temperature mosaic. Temperature mosaics were created with a single, thin, homogenous slab of the signature material at a specific temperature and density, then the spectra were graphed with respect to their temperatures. The temperature range inferred from the spectrum can be compared with the simulated temperature range of the plasma by viewing the DRACO output. If the physics in the simulation is complete, and if the simulated conditions reflect the experimental conditions, then the simulated spectra should resemble the experimental data.

### **Absorption Spectroscopy**

Absorption and emission lines are caused by bound-bound transitions of electrons in an atom, while absorption edges are caused by bound-free transitions of electrons. For bound-bound transitions, a photon of an energy that is equal to the energy of the transition has a high probability, depending upon optical depth, of being absorbed. At this photon energy, there is an increase in opacity, and this will result in an absorption line on the backlit spectrum. The areal density of the material and the cross-section of the atom determine the depth of the absorption line.

For a bound-free transition, a photon of an energy that is equal to or greater than the minimum bound-free transition energy has a higher chance of being absorbed. This is just the photoelectric effect. If the photon energy is greater than the transition energy, this will give the freed electron some extra kinetic energy. The opacity increases abruptly at the transition energy and then drops with higher energies. As a result, the absorption spectrum of an edge drops at the transition energy and slowly increases back to the intensity of the backlighter. The depth of the drop depends the cross section, which is inversely proportional to the square of the shielded nuclear charge.<sup>5</sup>

## Plasma Images

Plasma images were simulated for a target consisting of two strips of plastic, each 10  $\mu\text{m}$  thick and 60  $\mu\text{m}$  high and of indefinite length in the third dimension, placed against one another to make a target 20  $\mu\text{m}$  thick. The laser irradiated one side of the target nonuniformly to cause hydrodynamic perturbations that seed the Rayleigh-Taylor instability.<sup>6</sup> In Spect3D, the thickness in the third dimensional direction was changed to 0.27 cm to cause sufficient absorption to produce a significant contrast in the image. The images were taken at 1.6 ns after the beginning of the pulse. A figure of the setup of the experiment is shown in Figure 1a. All images were backlit with a Planckian blackbody radiating at a temperature of 2 keV.

The purpose of the images was to determine the completeness of the atomic models that were used for each simulation. A relatively complete model of the atom is necessary to represent all the important atomic processes that occur. Each image shows the relative opacity of each part of the material integrated over all frequencies,<sup>7</sup> since the depth is a projection of the two-dimensional simulation. The images were taken from a sideways view of the plastic but were then rotated counterclockwise to make the laser irradiation at the top of the image. The nonuniformities in the laser causes the perturbations at the top of the target in the image. The part of the target furthest away from the laser is cool, and it shows the most differences between complete and incomplete atomic models.

Using the image of a non-DCA (nDCA) opacity table as a guide, shown in Figure 2a, comparisons between different atomic models can be made. The table results will be used as the standard because it was created with the most complete model. DCA stands for Detailed Configuration Accounting, with which Spect3D calculates opacities, emissivities and cross sections based on an atomic model, while with nDCA, Spect3D reads off a table of opacities and emissivities. Each model has a certain number of configurations, and the user selects the ones to be used. The model with the least number of configurations has the worst agreement with the opacity table, where the bottom of the image is very transparent. However, as more configurations are added, the image looks closer and closer to the image of the table, which is opaque at the bottom. As more and

more configurations are added to the atomic model, there will be an increase in the number of possible transitions between each of the configurations. As a result, if the average cross section increases, the opacity increases, and the bottom of the image becomes more opaque.

In Figure 2b, the image is derived from a 17-configuration DCA carbon atom, where most of the levels are allocated to the He-like isoelectronic species, which has two electrons. The hydrogen atom model always has three lowest principal energy levels selected in all the DCA models. The backside of the plastic away from the laser is very transparent, because it is too cold for the He-like species to exist and the heat front has not yet arrived. Therefore, in the second model, shown in Figure 2c, more configurations were added to the lower-temperature species. The lower-temperature species are those with only a few electrons removed, and they exist at cooler temperatures. The backside becomes more opaque, but there is still a discrepancy. Another set of levels was added in to make a 158-configuration model. This image, in Figure 2d, shows that it is almost exactly the same as the tabulated model, because the back edge is more opaque.

After obtaining an atomic model that is very complete, a new goal is to make a more efficient model. Another atomic model of 106 configurations was created, where only the configurations for the 1s-2p and 2s-2p transitions are included. 1s-2p and 2s-2p transitions were chosen because 1s-2p are the most prominent in absorption, and because 2s-2p fill up vacancies in the 2p shell. The 106-configuration image, Figure 2e, shows almost no difference between that and the 158-configuration model. There are fewer levels in the atom, which will result in a faster computational time when the simulation is run. This use of the images helped determine which atomic model for carbon is complete enough for an accurate representation of the opacity tables in the absorption images.

A calculation of efficiency was made, where each model was run to determine the amount of time it took for each simulation. This was done to determine if a DCA model is worth its cost in time. The results are summarized in Table 1. The incomplete models had times comparable to the table, but the complete models took much longer. The best model, the 106-configuration model, took about four times as long as the table did. Therefore, it is feasible to use the DCA models rather than the non-DCA tables. DCA models have better effective resolution for temperature, density, and frequency than non-

DCA tables, and they can be used to simulate full level kinetics, including photoionization and photoexcitation models, while the tables are either local thermodynamic equilibrium (LTE) tables or collisional-radiative equilibrium (CRE) tables.

Emission images are compared as well to support the accuracy of the absorption image. The emission image of the 106-configuration model is shown in Figure 3b, and that of the non-DCA table is shown in Figure 3a. The calculated emission image looks very much like the tabulated spectra. This shows that the 106-configuration model is probably complete for simulating plasma images.

Type	Configurations	Time (sec)
DCA	17	108
DCA	42	141
DCA	106	435
DCA	158	1002
nDCA	All included by PRISM	112

Table 1

### Plasma Spectra at a Definite Time

The next step was to get spectra of the target, by doping some of the backside plastic with aluminum. Aluminum is usually used as a signature layer material during OMEGA experiments, so aluminum absorption will be simulated. Aluminum and silicon spectra were modeled with LTE. CRE could not be used because the temperature-dependence of the collision strengths were tabulated over too narrow a range of temperature in the atomic database. The setup for all spectroscopy experiments is shown in Figure 1b. From the spectral data, the amount of doping necessary for observable absorption was tested. For silicon, a 20% doped sample shows observable absorption, while aluminum that is doped only 5% shows observable absorption. Since aluminum and silicon differ by only one nuclear charge, it is surprising that they are not more closely interchangeable. The reason for this disparity is still under investigation. The absorption graphs of aluminum, shown in Figure 4a, show the spectra for different

percentages of doped aluminum, and the absorption graphs of silicon are shown in Figure 4b. Too much aluminum could saturate the lines and distinct lines could mesh together.

The aluminum model used in this simulation included the initial and final configurations with transitions that had a  $gf > 0.05$  as described in Ref. 8.  $gf$  is the product of ground-state degeneracy and the oscillator strength. This model shows all of the prominent 1s-2p absorption lines. When a model was created with all the 1s-2p and 2s-2p absorption lines, the spectrum looked very similar to the one created by the model with  $gf_{Al} > 0.05$ . The model included 2s-2p transitions because that decreases the average number of vacancies in the 2p shell. As a result, this should lower the average absorption cross-section of the 1s-2p transition.<sup>9</sup> If more configurations of the form  $1s^2(2s2p)^{w-1}nl$  were added, where  $3 \leq n \leq 10$  and  $1 \leq l \leq 4$ , it would increase the average number of vacancies in the 2p shell by allowing the excitation of those atoms. Therefore, an increase in the average cross-section occurs at temperatures greater than about 10 eV, and an increase in absorption will result.<sup>10</sup> However, this was not done in the atomic model because of the time cost of increasing the number of configurations. The model with the  $gf_{Al} > 0.05$  was the best model to use for accuracy and efficiency. Nonetheless, missing configurations were found in this model, such as the K-edges of M-shell species and of cold aluminum, but they were later added. The silicon model was the same as the best aluminum model with the same configurations.

### **Time-resolved absorption spectra**

The next step is to make useful spectra from DRACO output. After obtaining the DRACO output files, Spect3D was used to make a space-integrated, time-resolved streak spectrum. In Figure 5a, the spectrum was created from a 1-D unperturbed simulation. The unperturbed simulation is a piece of 20  $\mu\text{m}$  thick plastic, with a signature layer of 1  $\mu\text{m}$  aluminum 9  $\mu\text{m}$  deep, irradiated uniformly with a laser intensity of 200  $\text{TW}/\text{cm}^2$  for 2 ns.<sup>11</sup> The initial shock comes at about 200 ps, but the DRACO output time frequency is 100 ps so the Spect3D results resolution is only 100 ps; therefore, exactly when the shock comes is not clear. At around 1.4 ns, the heat front warms the aluminum very quickly, all the way up to its hydrogen-like state in about 150 ps. The laser is uniform; therefore, there is only a small range of temperature that the aluminum occupies. As a result, each

L-shell species disappears in about 300 ps. In the perturbed run, whose spectrum is shown in Figure 5b, the target foil is nonuniformly irradiated with the same laser. The shock appears at about 200 ps. However, the heat front does reach the aluminum about 100 ps earlier. Also, because of the perturbation and the Raleigh-Taylor instability, there is a wide range of temperatures. As a result, the F-like and O-like states persist, in contrast to the unperturbed DRACO run, for about 500 ps, until the end of the simulation. The range of temperatures determined by the F-like through H-like is about 600 eV. A plot of the maximum and minimum temperature of the aluminum signature layer for the perturbed and unperturbed DRACO simulations are shown in Figures 6a and 6b respectively.

The perturbed spectrum can then be compared to a streak camera output from an experiment done by OMEGA,<sup>4</sup> in Figure 7b. However, only qualitative analysis can be done because the input parameters for the DRACO simulation were different from those of the OMEGA experiment. For the experiment, the laser intensity was  $400 \text{ TW/cm}^2$  for a duration of 1 ns.<sup>4</sup> In Figure 7a, the color scale has been adjusted so that the perturbed DRACO run looks like the experimental streak camera output. This is permissible because the streak camera output is uncalibrated. The shock of the DRACO simulation appeared at about 200 ps, while the shock of the experiment appears at around 100 ps. This is expected from the differing intensities of the lasers. There is less shock preheating in the simulation than the experiment. The K-edge shift in the experiment shows when the shock arrives. However, because there was no continuum-lowering model in Spect3D, the distinct K-edges of magnesium-like and sodium-like species appear with the shock. Because of differences in input parameters, there was a later heat front arrival in the simulation. The main heat front heats the aluminum quickly, bringing up higher ionized states. In the simulation, heating goes all the way up to hydrogen-like, and fully-ionized aluminum as well, but in the experiment, it only goes up through beryllium-like. The higher temperature of the heat front could be a result of the use of CH as the signature layer in the DRACO simulation (changed to Al in the Spect3D simulation), as opposed to Al, which can radiate away heat.

## **Temperature Determination**

Hydrodynamically static LILAC<sup>12</sup> foils were simulated with Al foils 0.1  $\mu\text{m}$  thick at different temperatures and densities as input for Spect3D. Spectra at the various temperatures are arranged along a temperature axis. Absorption bands indicate the relative abundance of each L-shell and K-shell species through their relative opacity. The results are shown as temperature mosaics in Figure 8a for a density of one times solid and in Figure 8b for a density four times solid. These temperature mosaics can help experimentalists determine what temperature ranges occur in the signature layers. For example, if the fluorine-like species is present and the oxygen like species is not present at one times solid density, the temperature is between 20 and 30eV.

A mosaic for different densities could be made, so that an experimentalist, given an estimate of the densities from a hydro run, can determine the temperature range of the foil as a function of time from a time-resolved spectrum. The spectrum is much more dependent on temperature than on density, so if the spectrum is known and if only a rough estimate of the density is available, temperature can be found.

## Conclusions

Plasma images and spectra are outputs of the Spect3D radiation-transport post-processor. Backlit images can help determine the optical depth of the target. Spect3D can calculate opacities and emissivities based on an atomic model, and the plasma images help to determine which atomic model is the most complete and efficient. The completeness of the model is determined by how closely the image resembles the image of a table of opacities and emissivities obtained from a model known to be complete. The efficiency of the model can be determined by the run time of each model.

Plasma spectra can help determine the necessary amount of aluminum in a signature layer to obtain observable absorption. They also can create temperature mosaics for experimentalists to determine the temperature ranges of the signature layer from streak camera spectra. Most importantly, Spect3D can create space-integrated, time-resolved spectra to compare multi-dimensional hydrodynamic simulated spectra with streak camera spectra from experiments. Spect3D is a powerful tool that will be used in the future to solve the radiation transfer problem, to determine the properties of laser-driven plasmas, and thus help improve the effectiveness of laser fusion.

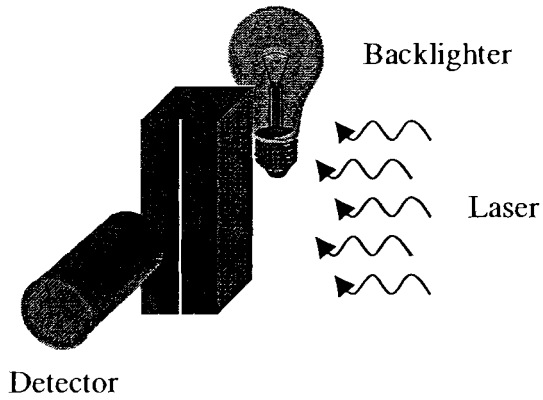
## References

- [1] J. J. MacFarlane, et al., SPECT3D Imaging and Spectral Analysis Suite, PRISM Computational Sciences, Inc., (2000).
- [2] DRACO hydrodynamic code, Laboratory for Laser Energetics, University of Rochester, (2000).
- [3] B. Yaakobi, R. S. Craxton, R. Epstein, Q. Su, "Areal-Density Measurement of Laser Targets Using Absorption Lines," *J. Quant. Spectrosc. Radiat. Transfer* **58**, 75-83 (1997).
- [4] T.R. Boehly, private communication.
- [5] G. C. Pomraning, *The Equations of Radiation Hydrodynamics* (Pergamon, Oxford, 1973).
- [6] R. S. Craxton, et al., *Scientific American* **255**, 68-79 (1986).
- [7] J. J. MacFarlane, SPECT3D Getting Started Manual (Version 1.3), PRISM Computational Science, Inc., Report # PCS-R-011.
- [8] C. Chenais-Popovics, C. Fievet, J. P. Geindre, J.C. Gauthier, E. Luc-Koenig, J. F. Wyart, H. Pépin, M. Chaker, "K  $\alpha$  absorption spectroscopy: Diagnostic of the radiative preheating of a laser-irradiated layered target", *Physical Review A* **40**, 3194-3208 (1989).
- [9] R. Epstein, "Satellite absorption lines and the temperature dependence of x-ray absorption features in high-temperature plasmas." *Physical Review A* **43**, 961-967 (1991).
- [10] J. Abdallah, Jr., R. E. H. Clark, J. M. Peek, "Excited-state  $1s-2p$  absorption by aluminum ions with partially filled L shells." *Physical Review A* **44**, 4072-4075 (1991).
- [11] R. Town, private communication.
- [12] LILAC hydrodynamic code, Laboratory for Laser Energetics, University of Rochester.

## Acknowledgements

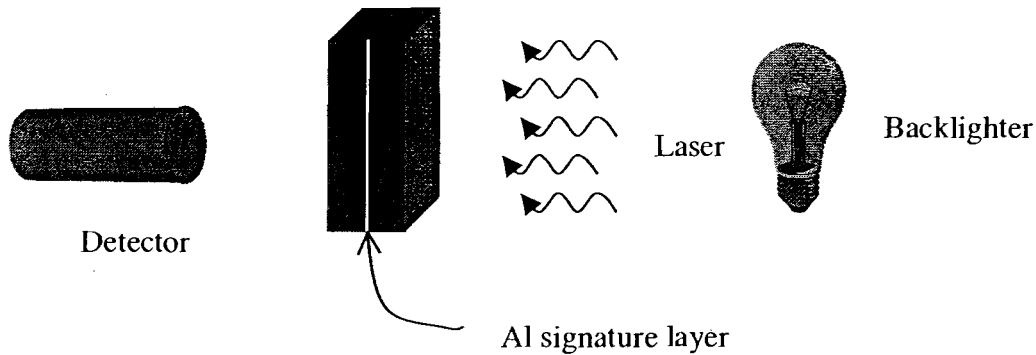
I would like to thank first and foremost, my advisor Dr. Reuben Epstein for mentoring me throughout this whole project. I would also like to thank Richard Town for providing me with all the DRACO runs that were used as input in the Spect3D, and Tom Boehly for providing the experimental data. Additional thanks goes to the other theorists of the

Theory and Computation Group at LLE: Radha Bahukutumbi, and Jacques Deleltrez; the people at PRISM Computational Sciences: Joe J. MacFarlane, Andy Thomas-Cramer, and Pei Zeng; the computer managers at LLE: Tony Brancato, David Keller, and Alan Shechter. Finally I would like to thank Dr. R. Stephen Craxton for giving me the opportunity to work here at LLE for this summer.



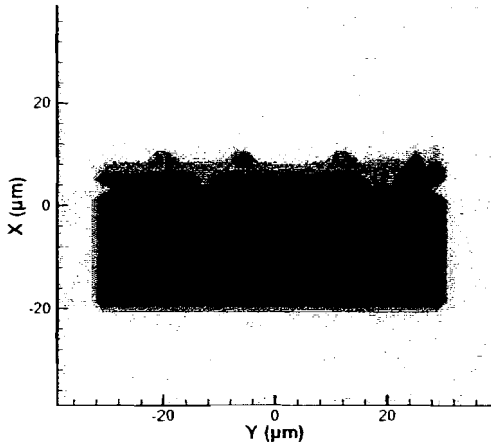
**Figure 1a**

This shows the setup of the simulation when modeling of the plasma images was done. The laser light is coming from the right, the backlighter is behind the target, and the detector is in front of the target. The backlighter is represented by a light bulb.



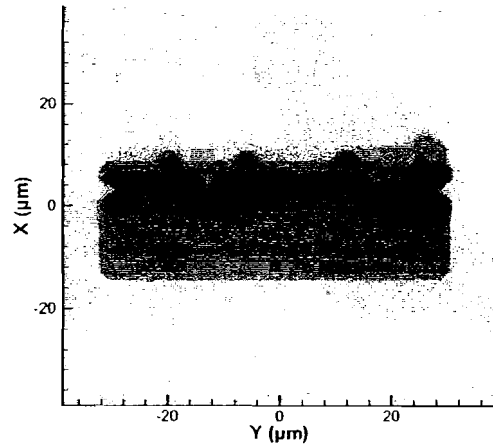
**Figure 1b**

This shows the setup of the simulation when the spectra of the targets were modeled. The laser light is still coming from the right, but the backlighter is also on the right, and the detector is placed on the left. In an actual experiment, the backlighter would be a piece of high-Z material. When a laser light shines upon it, it produces x-rays.



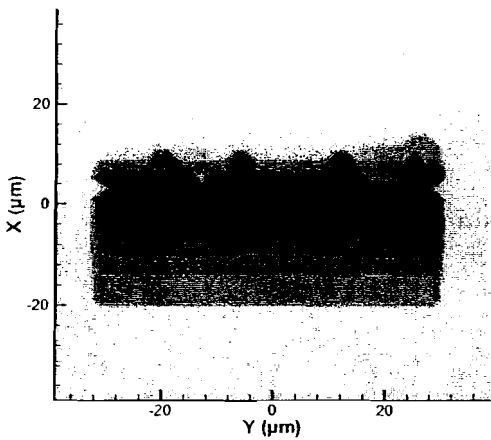
**Figure 2a**

This is the absorption image of a nDCA simulation. The bottom of the image is very opaque.



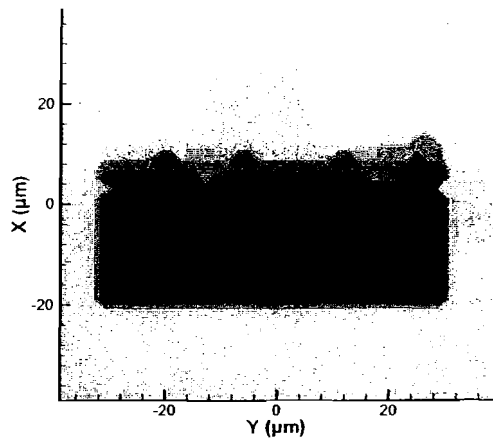
**Figure 2b**

This is the absorption image of the 17-configuration DCA model. The bottom of the image is very different from the nDCA model.



**Figure 2c**

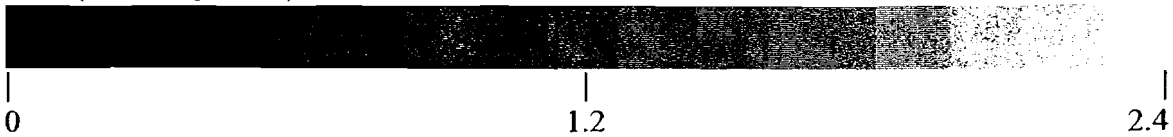
The image of the 42-configuration model looks better than the 17-configuration model as compared to the nDCA model.

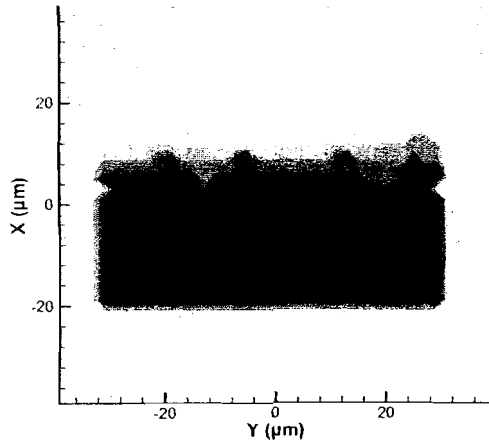


**Figure 2d**

This is the absorption image of the 158-configuration model, and it looks almost exactly like the nDCA model.

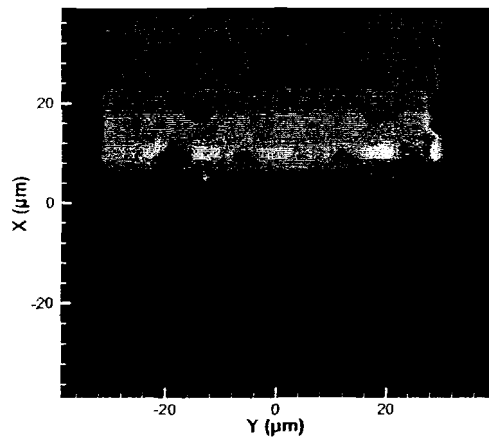
Absorption images:  
Flux ( $\times 10^{12}$  erg/cm<sup>2</sup>/s)





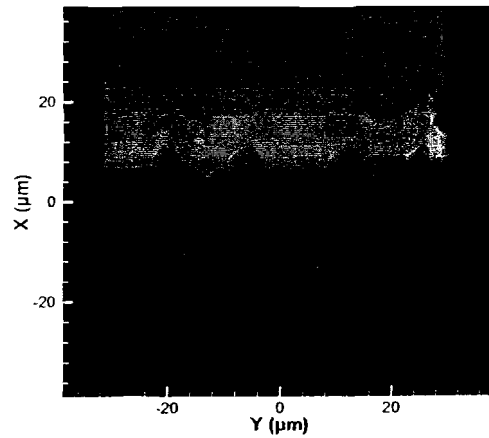
**Figure 2e**

This model, the 106-configuration one, is the best approximate of the nDCA model and is the most efficient.



**Figure 3a**

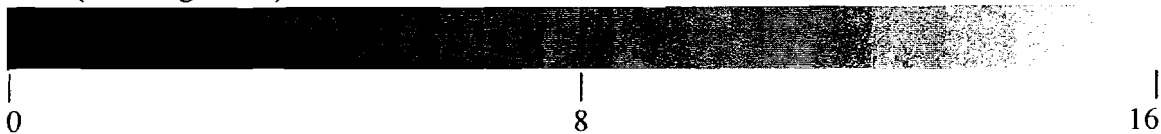
This is the emission image of the nDCA simulation. The emission comes from the hotter part of the plasma where the H- and He-like species exist.



**Figure 3b**

This is the emission image of the 106-configuration model. It looks very similar to the nDCA simulation.

Emission images:  
Flux ( $\times 10^8$  erg/cm<sup>2</sup>/s)



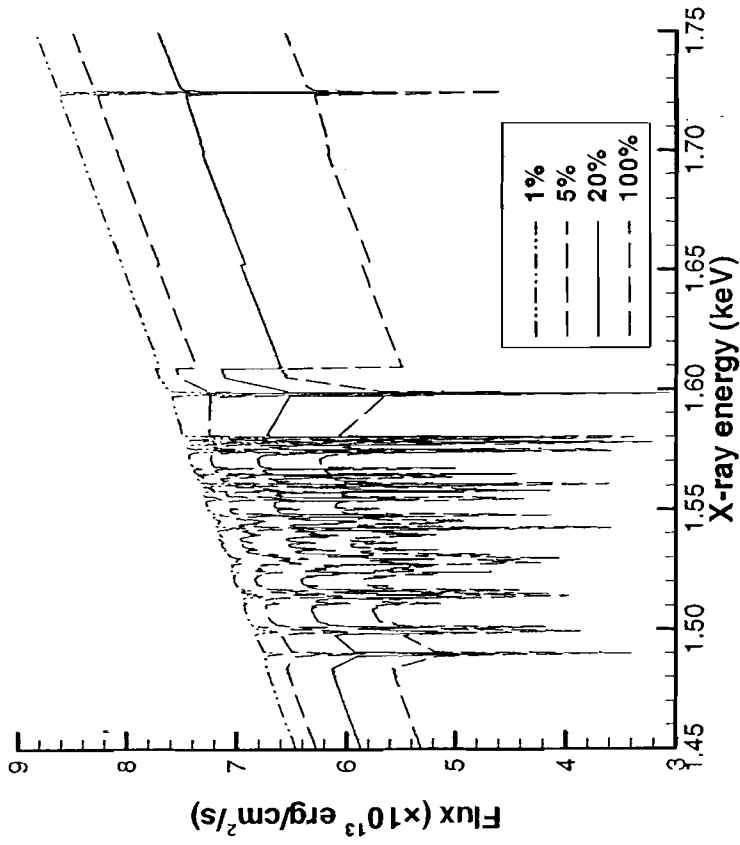


**Figure 4a**

This figure shows absorption spectra with different doped amounts of Al in a CH layer. When there is only a few percent of aluminum, the absorption spectrum is relatively small, but as the concentration of aluminum is increased, saturation begins to occur.

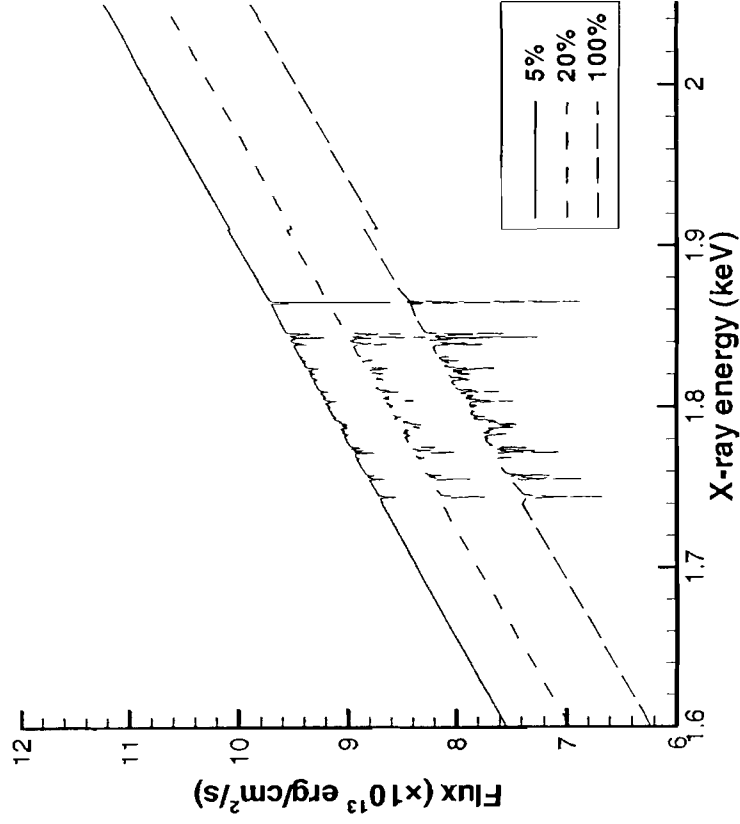


**Figure 4b**

This figure shows absorption spectra of different doped amounts of Si in a CH layer. The absorption of Si is much less than the absorption of Al, for reasons under investigation for the moment. However, an observable spectrum can be seen with a doped amount of 20% Si.

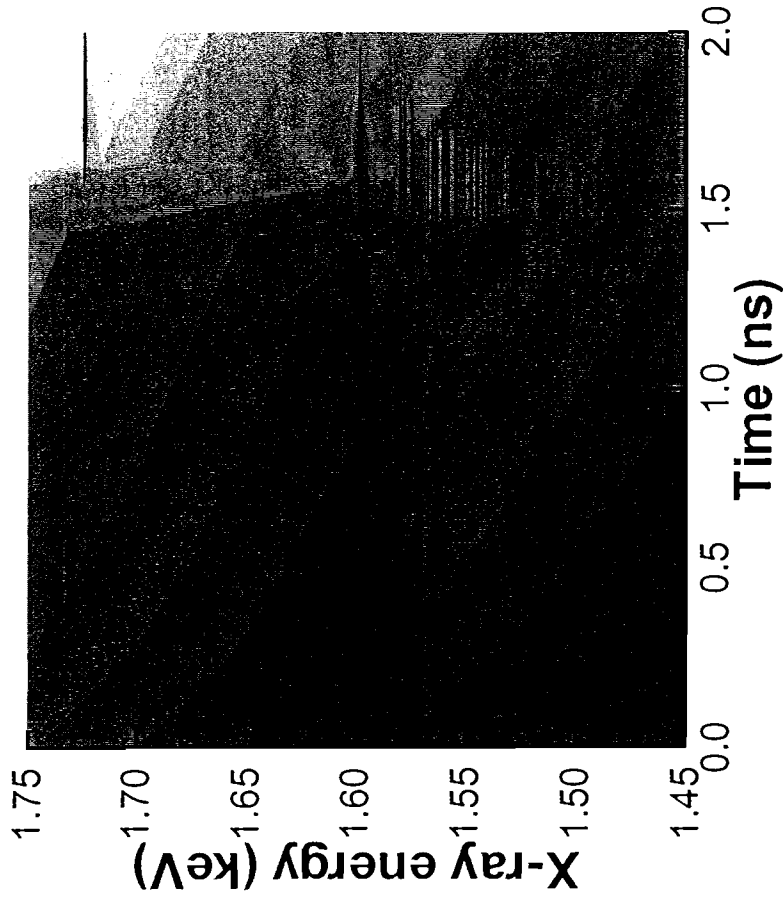


**Figure 5a**

A simulated space-integrated, time-resolved spectrum of a uniformly irradiated piece of plastic with an aluminum signature layer. Notice the lines of the different species disappear after a short time. They show that the temperature range of aluminum is relatively small.

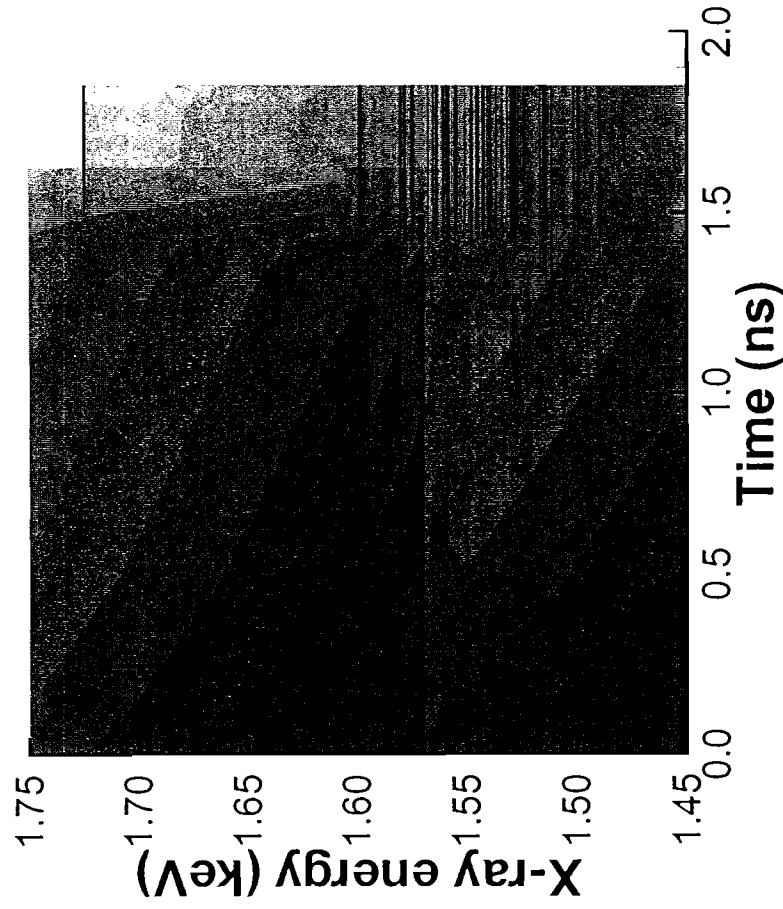
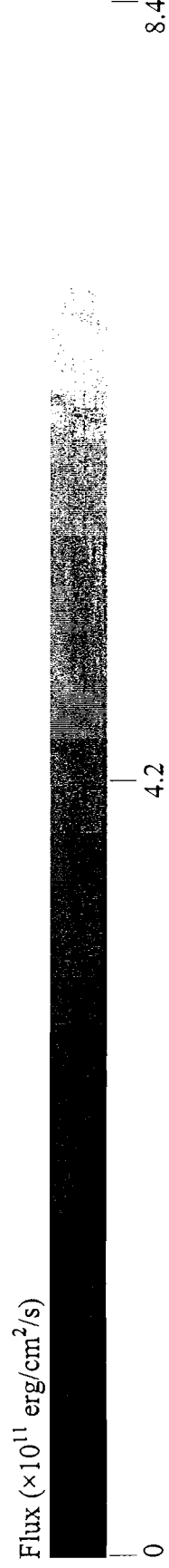


**Figure 5b**

A similar simulation is run with a non-uniformly irradiated target. Each of the ionization species persists until the end of the simulation to show the aluminum has a wide range of temperature. Also the heat wave arrives earlier due to the perturbation.



4.2

8.4

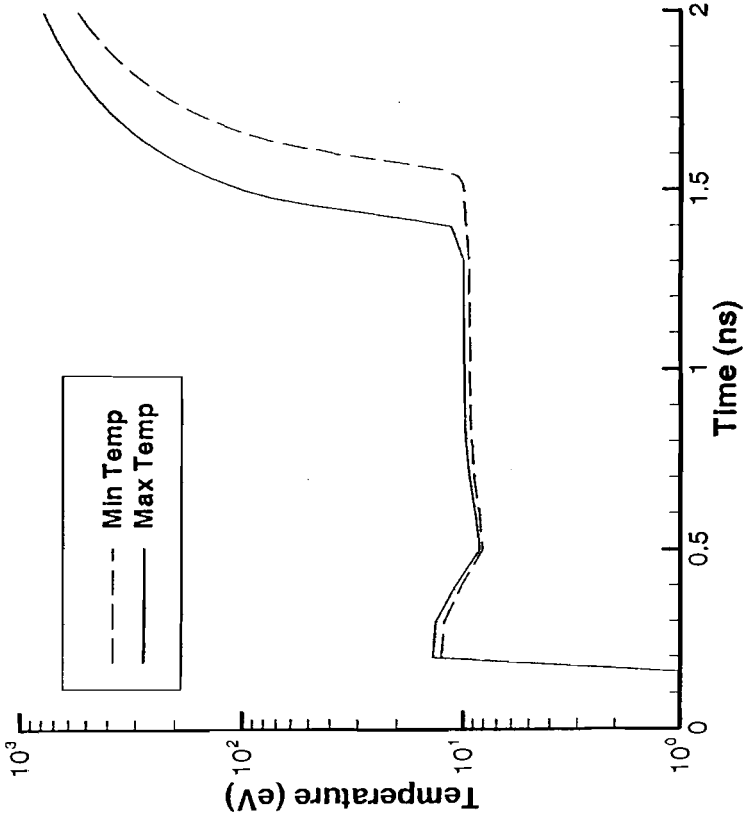


Figure 6a

A temperature profile of the aluminum signature layer. This is the unperturbed simulation, and it shows that the temperature range after the heat front arrival is small.

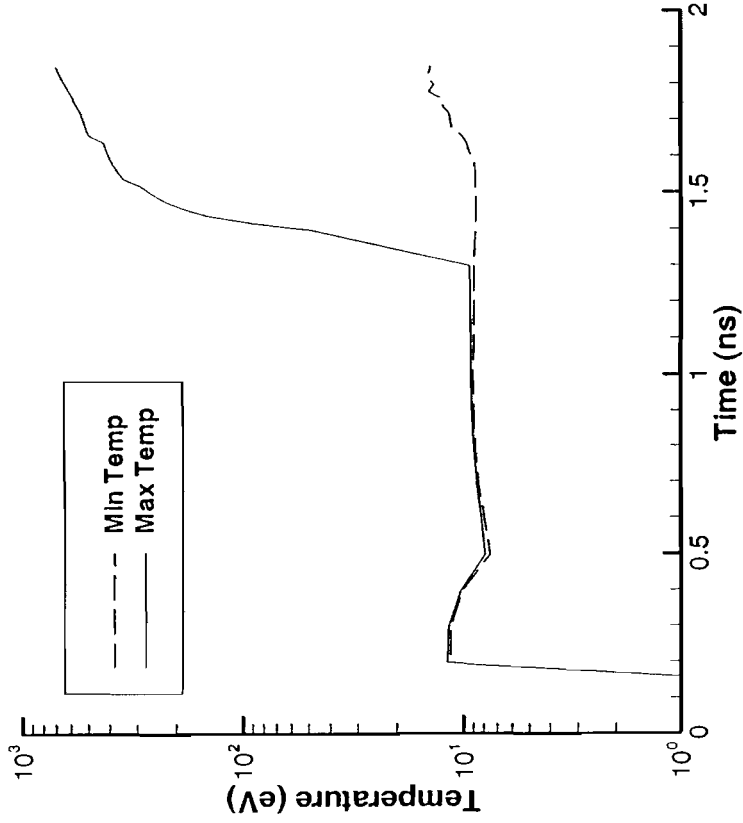


Figure 6b

A temperature profile of the perturbed simulation. Note that the minimum temperature stays relatively constant after the heat front arrives, while the maximum temperature increases.

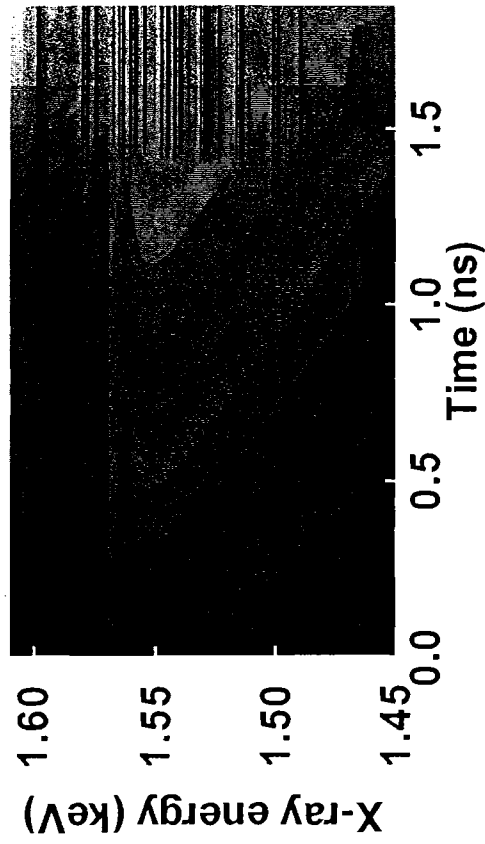


Figure 7a

This is the same as Figure 5b, but the colormap has been changed to match that of the experimental streak camera. The axes have also been changed to facilitate comparison between the images. The K-edges of M-shell species appear with the shock at  $\sim 200$  ps, and the L-shell and K-shell species appear when the heat front arrives at  $\sim 1.3$  ns.

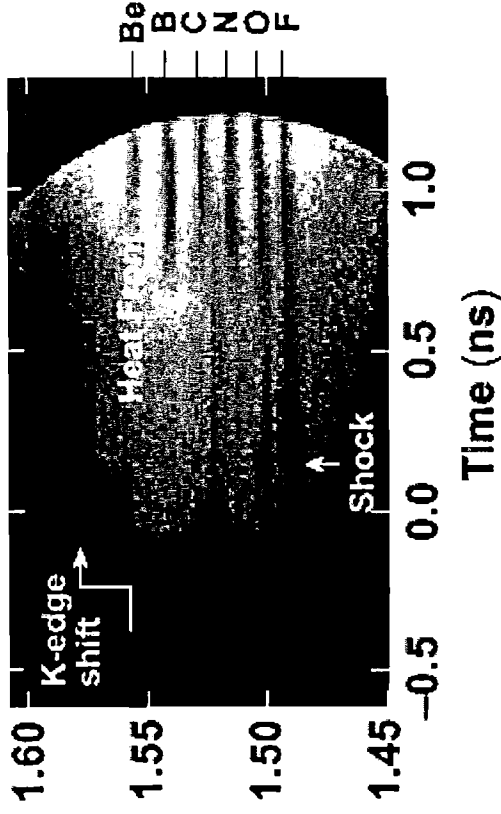
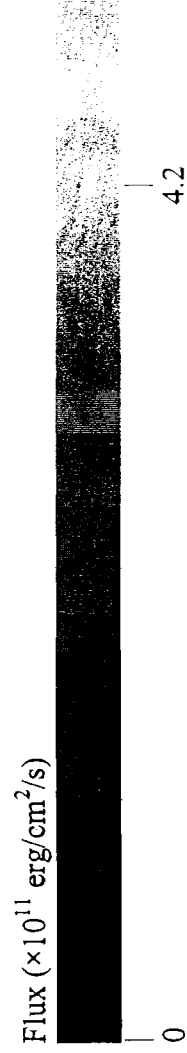


Figure 7b

This is an experimental spectrum of an OMEGA experiment. The shock arrives at  $\sim 100$  ps heating the plasma to F- and O-like, and the heat front arrives at  $\sim 800$  ps showing up to Be-like species.



4.2

8.4

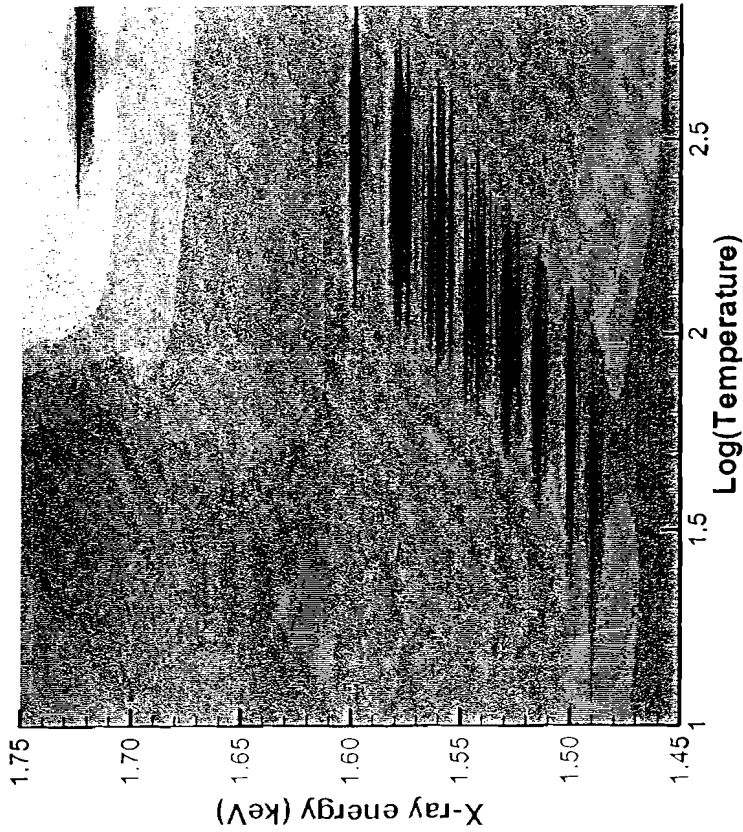


Figure 8a

A temperature mosaic of a simulated absorption spectrum for one times solid density aluminum. The temperature range is from 10 to 700 eV, and it shows the appearance and disappearance of most of the L-shell and K-shell species

Flux ( $\times 10^{11}$  erg/cm<sup>2</sup>/s)

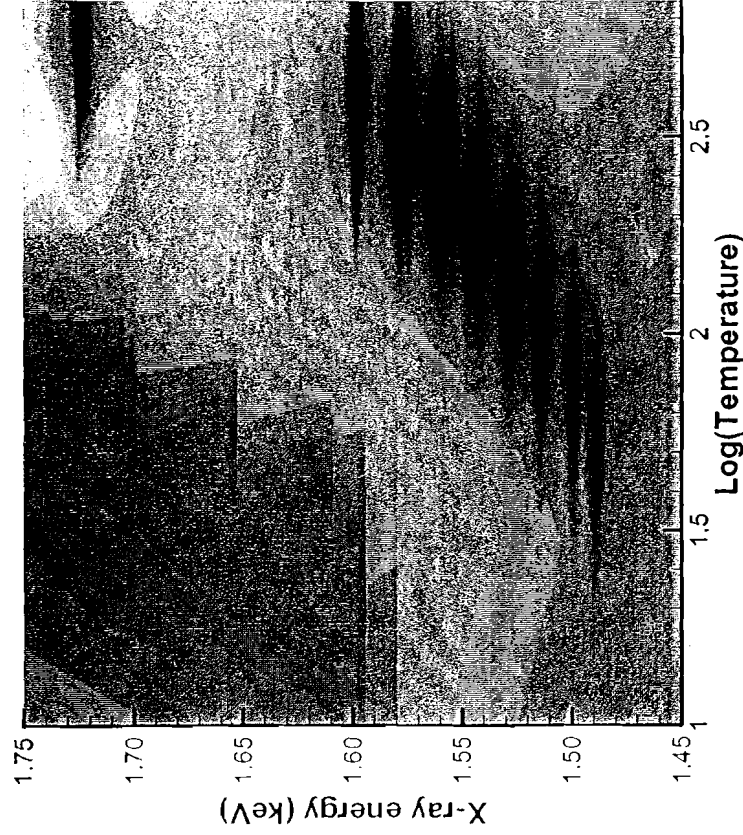


Figure 8b

A temperature mosaic of a simulated absorption spectrum for four times solid density aluminum. The temperature range is 10 to 700 eV. The absorption spectrum is highly saturated since the aluminum is denser.